Geomorphology 214 (2014) 114–127

Contents lists available at ScienceDirect

Geomorphology

journal homepage: www.elsevier.com/locate/geomorph

Coseismic landsliding during the M_w 7.1 Darfield (Canterbury) earthquake: Implications for paleoseismic studies of landslides

Timothy Stahl [a,*], Eric L. Bilderback [a,b], Mark C. Quigley [a], David C. Nobes [a], Chris I. Massey [c]

[a] Department of Geological Sciences, University of Canterbury, PB 4800, Christchurch 8140, New Zealand
[b] United States National Park Service, Geologic Resources Division, P.O. Box 25287, Denver, CO, USA
[c] Institute of Geological and Nuclear Sciences, PO Box 30368, Lower Hutt, New Zealand

ARTICLE INFO

Article history:
Received 4 September 2013
Received in revised form 3 March 2014
Accepted 6 March 2014
Available online 19 March 2014

Keywords:
Paleoseismology
Landslide
Coseismic
Ground cracks

ABSTRACT

The head scarp of the Harper Hills landslide consists of ground cracks with vertical displacement and extension that opened during the 2010 Darfield (Canterbury) M_w 7.1 earthquake. The geomorphology of the cracks, regional geology and ground penetrating radar indicate that the landslide formed by bedding-controlled translation and joint-controlled toppling, and suggest incipient deep-seated movement. Crack depth and displacement along the head scarp vary along the ridge; maximum values are located where the head scarp is closest to the local ridge line. Increased seismic shaking due to topographic and geometric amplification of seismic waves is suggested as an explanation for this relationship. An excavation across the head scarp revealed no evidence of prior slip events over a time period that is likely to exceed the return period (1000–2500 years) of peak ground accelerations experienced at this location in the Darfield earthquake. We suggest that specific seismologic attributes of the Darfield earthquake may have influenced the location of landsliding in this instance. Studies of paleolandslides must consider crack preservation potential as well as complex source/site effects that may complicate estimates of acceleration return periods from the subsurface investigation of individual landslide head scarps.

1. Introduction

Earthquake induced landslides are a major hazard in susceptible regions. The understanding of seismic conditions under which landslides are triggered is assisted by empirical data from past landslides. Characteristics of strong ground motion may be ascertained by combining geological and geomorphologic studies with simple back-analysis models of slope stability (Jibson and Keefer, 1993; Jibson, 1996, 2011). These studies are of interest to paleoseismologists because landslides have the ability to provide a history of earthquake-induced strong ground motion at a site independent of fault studies.

Where deep-seated landslides have been preserved in the landscape, geomorphic mapping and trenching can yield information on ground failure (e.g. Nikonov, 1988; Nolan and Weber, 1992; McCalpin and Irvine, 1995; Nolan and Weber, 1998; Onida et al., 2001; McCalpin and Hart, 2002; Gutiérrez et al., 2010a; Hart et al., 2012; Moro et al., 2012; Carbonel et al., 2013). Trench studies allow determinations of landslide kinematics and movement rates that can help distinguish whether motion is episodic or progressive (Agliardi et al., 2001; Johnson and Cotton, 2005; Gutiérrez et al., 2008, 2010b). Without a detailed inventory of mechanical rock properties, ground water conditions, and a range of possible seismic inputs and site-response characteristics, unambiguous evidence of a seismic origin is often difficult to obtain. In areas of active faulting, the determination of a seismic or aseismic origin, and the causative fault source, has a significant impact on determining hazard.

In this paper, we present a geomorphic and subsurface study of ground cracks that opened coseismically during the 2010 Darfield earthquake in New Zealand. Trenching and ground penetrating radar (GPR) are used to investigate the kinematics, morphology, and failure mechanism of the landslide. We conclude with suggestions for incorporating subsurface records of strong ground motion from landslides into paleoseismic analyses.

2. Geologic and tectonic setting

2.1. Darfield earthquake

The M_w 7.1 Darfield (Canterbury) earthquake (henceforth the Darfield earthquake) in New Zealand was caused by rupture on a series of previously unrecognized faults underlying the low relief Canterbury Plains (Fig. 1; Beavan et al., 2010; Quigley et al., 2010; Gledhill et al., 2011; Beavan et al., 2012; Elliott et al., 2012; Quigley et al., 2012). The earthquake initiated on the steeply dipping, reverse Charing Cross fault which triggered predominantly strike-slip motion on three to four E–W to NW–SE striking Greendale Fault segments. Two other strike-slip faults intersecting the main Greendale Fault traces and a

* Corresponding author. Tel.: +64 212861202.
E-mail address: stahl.geo@gmail.com (T. Stahl).

http://dx.doi.org/10.1016/j.geomorph.2014.03.020
0169-555X/

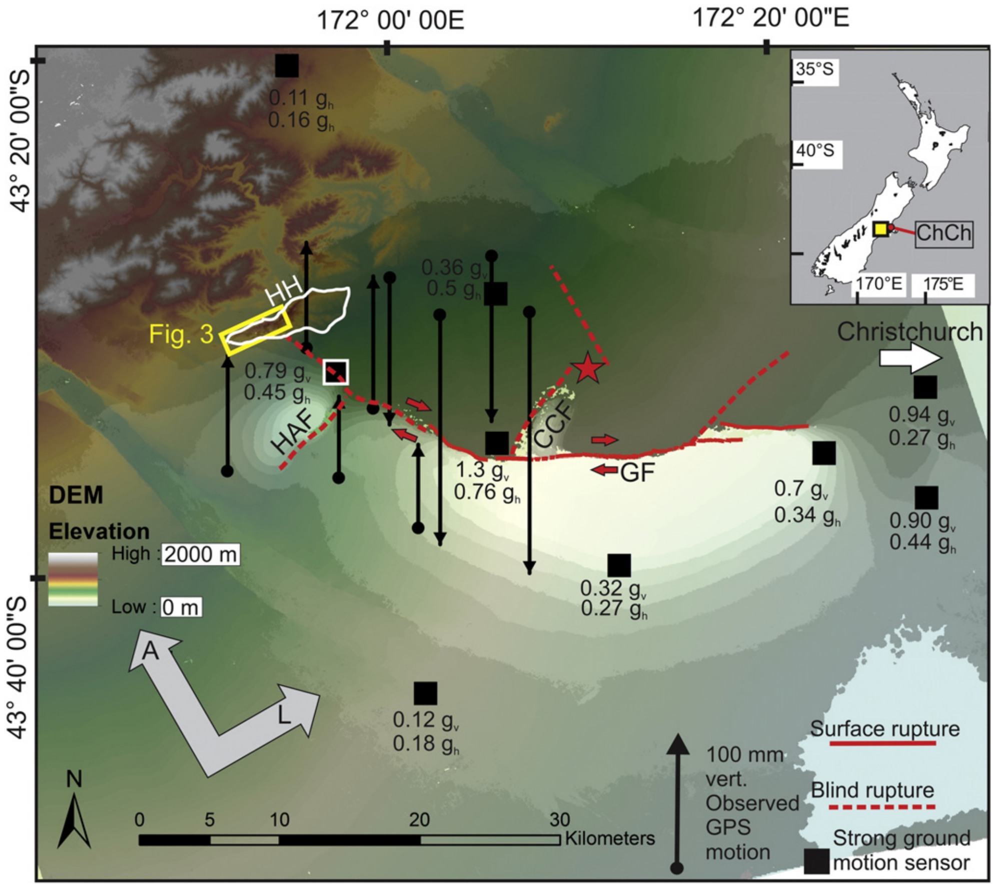

Fig. 1. Map and study site location. 15 m Digital Elevation Model (DEM) showing (i) Location of faults involved in the 2010 Darfield earthquake: Greendale fault (GF), Hororata anticline fault (HAF), Charing Cross Fault (CCF) and other unlabeled structures from Beavan et al. (2012); ii) DInSAR interferogram showing relative motion of faults with respect to the satellite heading direction (A) and satellite look direction (L). Lighter areas moved towards the satellite (up or in the direction of L), and darker areas moved away; iii) selected GPS stations with absolute motions; iv) selected strong ground motion sites with vertical and horizontal PGAs reported from Bradley (2012). White outlined station is HORC (see text for discussion); and v) location of the Harper Hills (white outline on the DEM) and the field area (Fig. 3).

second high-angle, blind reverse fault to the West (the Hororata Anticline Fault, HAF) also ruptured (Beavan et al., 2012; Elliott et al., 2012; Jongens et al., 2012). Differential interferometric synthetic aperture radar (DInSAR) (Fig. 1) highlights the relative motions of the major fault planes towards (lighter) and away from (darker) the line of sight of the recording satellite (Beavan et al., 2010). GPS measurements and other survey techniques indicate a maximum of 1.4–1.6 m vertical, normal displacement on the western segment of the Greendale Fault at the surface and 0.4 m uplift on the intersecting HAF, both NW-side up (Beavan et al., 2010, 2012; Duffy et al., 2013).

Peak ground accelerations on the Canterbury Plains reached a maximum of ~1.3 times that of gravity (g) near the Greendale Fault (Gledhill et al., 2011; Bradley, 2012). Finite-element modelling of uninstrumented ridge-tops in the Port Hills (east of the Greendale Fault) where boulders were displaced in the Darfield earthquake indicates frequency-dependent amplification of PGAs of up to 80% greater than at the base of the hills (Khajavi et al., 2012). The multiple-fault rupture contributed to complex and varying waveforms at recording stations, though in general accelerations recorded within 25 km of the Greendale Fault all exceeded 0.1 g (horizontal and vertical over 0.01–10.0 s period) with 5–95% significant durations of 20–30 s (Bradley, 2012).

2.2. Harper Hills

The Harper Hills are located 20 km west of the epicenter of the Darfield earthquake and 9 km northwest of the up-dip projection of the HAF (Fig. 1). The south-western 5 km of the E–NE trending strike-ridge is located on the hanging wall of both the HAF and the subsurface extension of the Greendale Fault (see Fig. 1). The nearest strong motion seismometer ('HORC', Hororata School, Fig. 1) recorded a peak vertical acceleration of 0.79 g and a peak horizontal accelerations of 0.45 to 0.51 g (using methods of Bradley, 2012 and GeoNet for horizontal accelerations, respectively). The 5–95% significant duration was markedly shorter for HORC (8.7 s) compared with stations further away from the causative faults (Bradley, 2012). Horizontal accelerations were strongest in W–NW/E–SE directions with the highest vertical accelerations recorded in the NW and SE quadrants (Fig. 2; 0.1 Hz high-pass filtered data currently held by GeoNet).

The Harper Hills strike-ridge is asymmetric with a steep scarp slope (40–70°) and gentle dip slope (20–40°) defined by joint and bedding planes, respectively (Figs. 3 and 4). It is one of the easternmost topographic highs in the foothills of the Southern Alps despite the relatively subdued 210 m of relief. The regional geology consists of SE-dipping Cretaceous–Tertiary sandstones, volcanics, and locally-mined beidellite–montmorillonite–bentonite units of the Burnt Hill Group (Carlson et al., 1980; Browne, 1983). On the scarp slope, jointed blocks of the Upper Miocene Harper Hills Basalt can be observed conformably overlying well-bedded Sandpit Tuff. Pliocene gravels overlie the Burnt Hill Group on the dip slope of the field area. North-east of the field area, Forsyth et al. (2008) mapped undifferentiated Quaternary landslide deposits along the dip-slope below the Harper Hills Basalt (Fig. 3). The Hororata Fault (a different structure than the HAF, which ruptured in the Darfield earthquake, Fig. 1) bounds the north-eastern section of the Harper Hills (Fig. 3).

The Harper Hills Basalt is identifiable as a prominent scarp along the length of the Harper Hills. Rolling hills with ~10 m scale local relief,

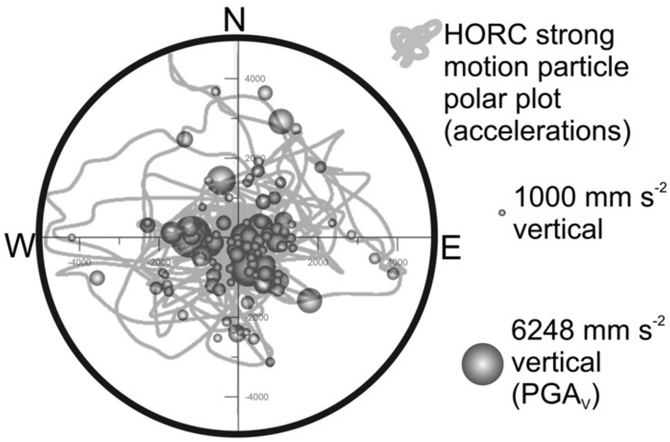

Fig. 2. Local ground motion characteristics. Strong motion polar plot at Hororata School (HORC) with i) two-component horizontal accelerations and ii) largest vertical accelerations scaled to magnitude and located according to its two horizontal components (data from GeoNet).

slope-parallel drainages and numerous swales dissected by small streams characterize the dip-slope of the Harper Hills. Arcuate to curvilinear breaks in slope, hummocky terrain and several shallow slope failures are indicative of ongoing landsliding. Muirson (2003) identified a bedding-controlled, deep-seated landslide north of the field area in this study. The Chalk Hill Clay, a bentonitic unit, and the overlying Sandpit Tuff were identified as possible failure planes. The former has a residual internal friction angle (21°) less than the regional slope (~30°) (Muirson, 2003). Historical photos show that the landslide is older than 50 years, but could be much older.

3. Harper Hills coseismic landslide

Curvilinear ground cracks parallel to the ridge-line of the Harper Hills were documented two days after the Darfield earthquake (Figs. 3 and 4). Landowners stated that the cracks had opened during or within 2–3 h of the main shock (4:35 am NZST) as the features were first observed at dawn. A small stock pond (seen in Fig. 4B) was reported to have drained in an aftershock within 2 days of the main shock, perhaps implying a second phase of displacement on the cracks. The ground cracks displaced farm tracks in a few locations and tension from surface extension caused fence wire to snap in at least one location and tighten at several others. Damage to infrastructure was otherwise minor.

Cracks were mapped on the ground using differential GPS (dGPS) aided by aerial reconnaissance (Fig. 4A–F). The cracks occur intermittently along the southern Harper Hills for 2.5 km, with the south-westernmost 1 km containing over 75% of the features. Cracks occur at 340–380 m elevation, but most commonly at 370–380 m. The longest continuous features are approximately 120 m long and occur at the south-western and north-eastern extremities (Fig. 4C and E, respectively). In places, the cracks traverse the local slope but remain parallel to the average strike of the Harper Hills ridge line (i.e. cut across topography; Fig. 4A). On the top of interfluves in the central region of the landslide, displacement is relatively small and often expressed as fissures that straddle surface cobbles (Fig. 4F). There was no surface break at the foot of the Harper Hills, though a 27 m long crack was observed 460 m SE (down-slope) of the head scarp. The best expression of this crack was on a road which was

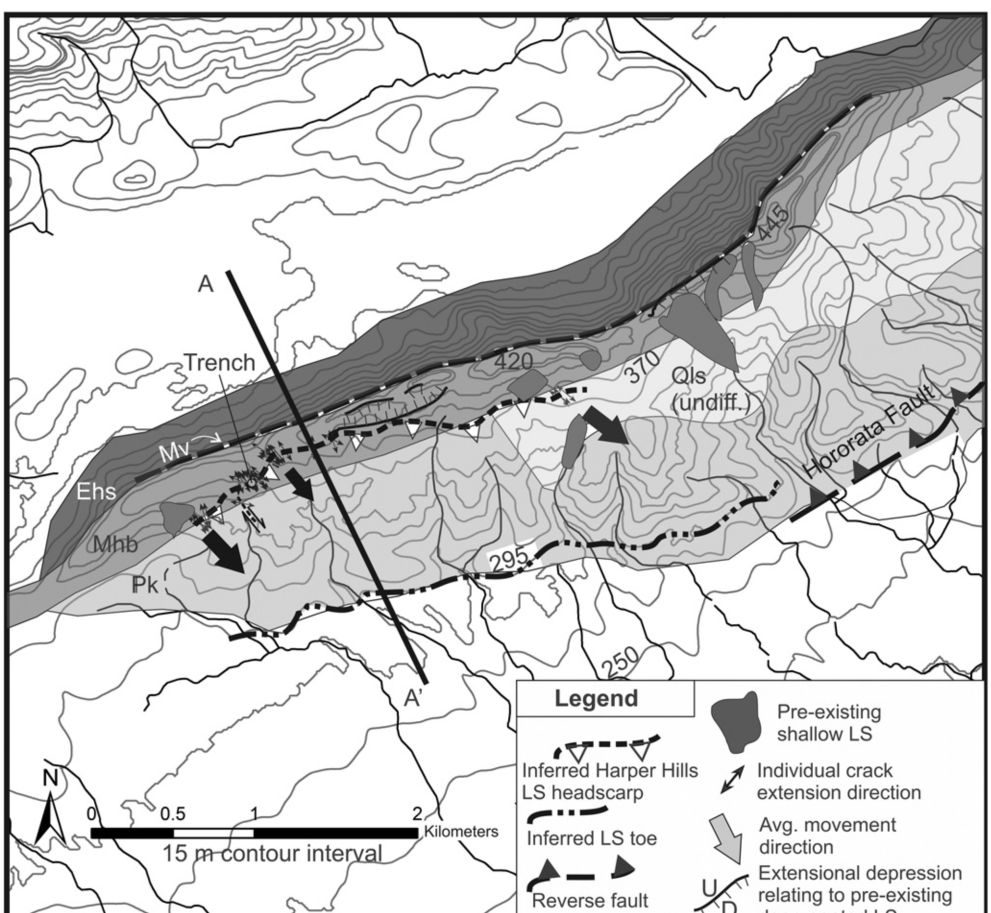

Fig. 3. Geologic and geomorphic map of the field area. LS (in the legend): Landslide; Ehs: Homebush Sandstone; Mv: Undifferentiated volcanics (Sandpit Tuff & Chalk Hill Clay) with minor limestone; Mhb: Harper Hills Basalt; Pk: Kowai Gravels; Qls: Undifferentiated Quaternary landslide deposits. Based on Forsyth et al. (2008). Cross-section A–A' shown in Fig. 9.

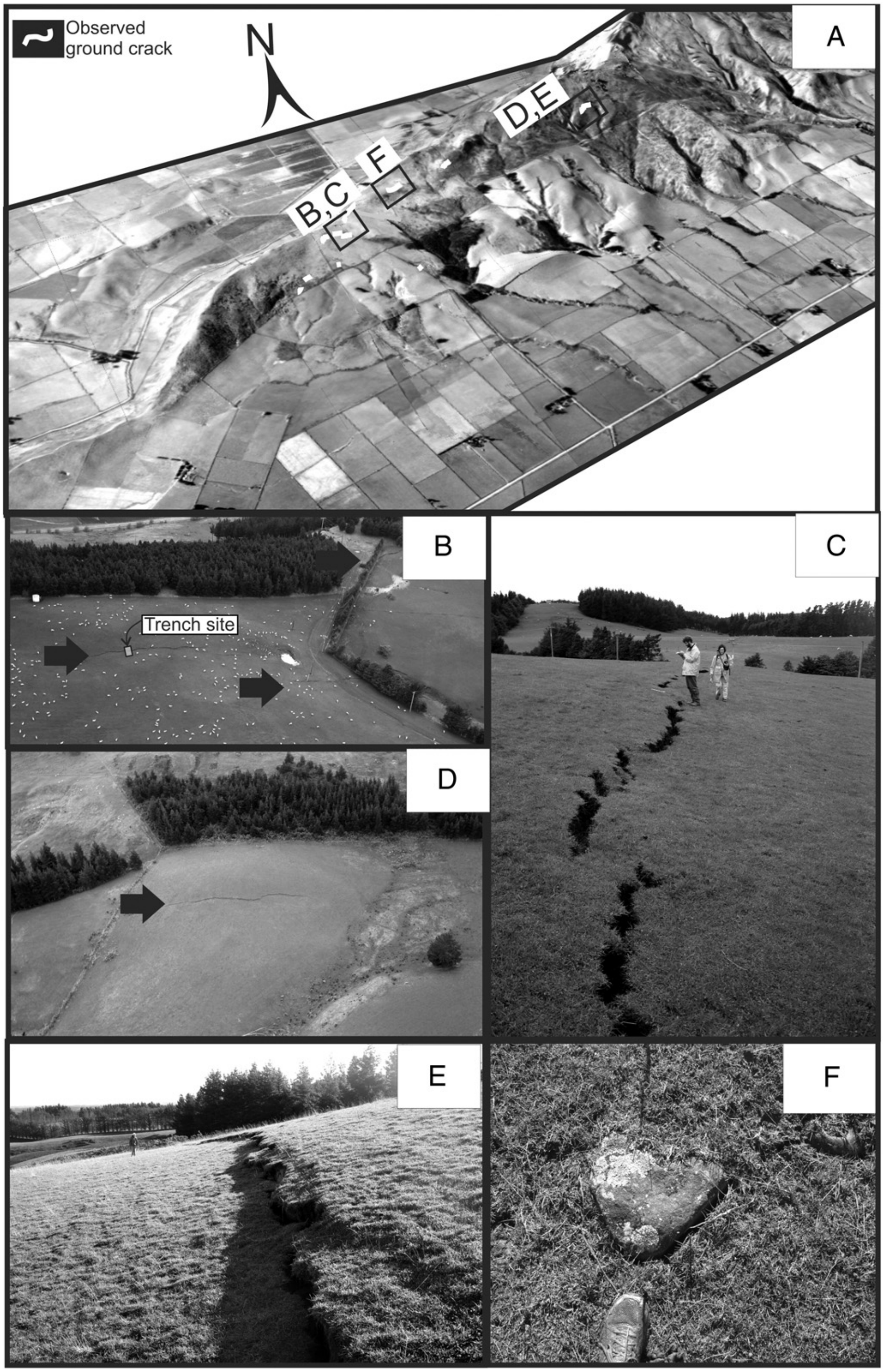

Fig. 4. Ground crack map and field photos. A) Aerial photography overlain on a 15 m DEM showing hill geometry and location of mapped ground cracks shown as short white lines. B–F) Field photos of ground cracks (See text for discussion).

re-graded soon after the earthquake, but displacement was observed to be small in comparison to the head scarp region.

Measurements of crack depth, extension, vertical displacement and movement direction were taken at 41 points along the length of the cracks. The most pronounced cracks are located in a 400 m stretch on the south-western end of the landslide where 73% of the cumulative net displacement is recorded over 16% of the along-strike distance. The largest net displacements were measured on the cracks with the greatest fissure depth, and these are typically situated closest to the Harper Hills ridge-line (Fig. 5). Monitoring arrays consisting of two to three wooden pegs were placed across the features at seven locations. Over the course of 2 years, the pegs were re-measured five times using a tape measure, and no further relative displacement across the cracks was observed.

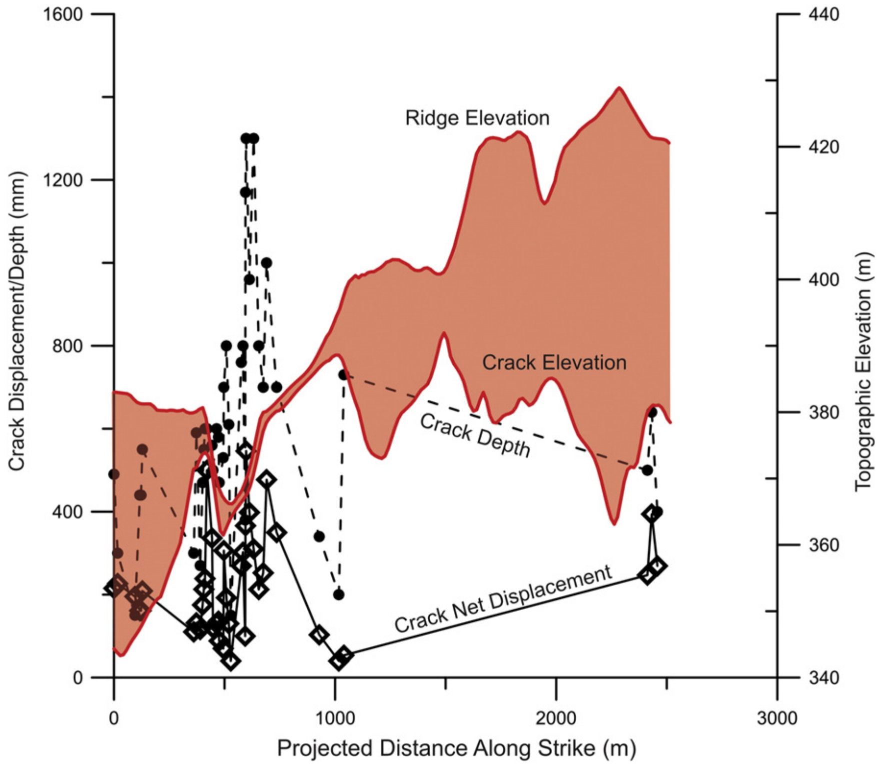

Fig. 5. Measurements of ground deformation. Crack net displacement (open diamonds, solid line) and depth (filled circles, dotted line) in mm plotted against projected distance along the landslide. Ridge to crack relief envelope (red) shows that cracks with the most displacement/depth generally occur nearest the ridge-top (i.e. where the envelope is thinnest). Where cracks were discontinuous across the slope, the lower boundary of the relief envelope was determined by connecting straight elevation profiles (in map view) to the next feature.

Crack extension directions were weighted by net displacement and compared to the regional structural geology trends and slope (Fig. 6). Bedding and joint measurements were taken NW of the head scarp from outcrops of the Harper Hills Basalt overlying the Sandpit Tuff. Bedding measurements NE of the field site reveal a consistent strike and dip along the length of the Harper Hills (Carlson et al., 1980; Muirson, 2003). Poles to the dominant joint set (steeply NW-dipping, $n = 9$) and bedding planes (SE-dipping, $n = 4$) match the average

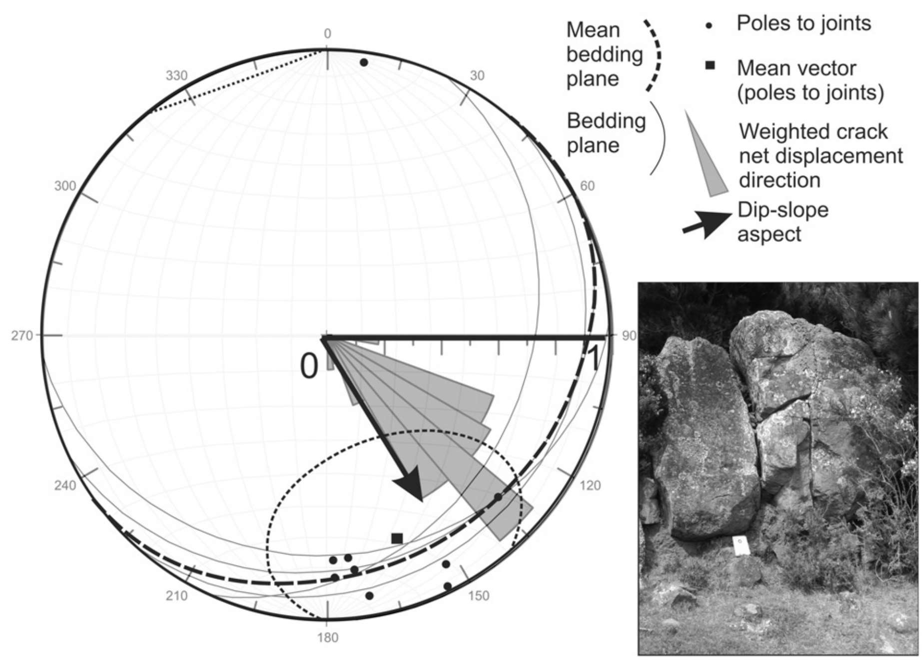

Fig. 6. Structural and kinematic measurements. Combined rose diagram and lower-hemisphere equal area projection showing i) Crack displacement direction weighted for net displacement; ii) dip-slope aspect (down-slope direction); iii) orientations of bedding derived from an outcrop in the lower right corner (thin lines) and average bedding plane orientation (thick dashed line); iv) poles to the dominant set of joints (filled circles) with the mean vector (square) and 95% confidence cone (dashed). Outcrop at bottom right shows the Harper Hills Basalt overlying the Sandpit Tuff. Bottom of the field notebook is situated on a bedding plane contact, dipping shallowly into the page, and the cover is parallel to the dominant joint set, dipping steeply out of the page.

orientation of the crack extension direction and DEM-derived aspect of the dip-slope. Crack extension direction best coincides with dip-direction of bedding (135° and 144°, respectively), though the 95% confidence interval of poles to joints and the dip-slope aspect both overlap the crack extension directions.

Some small, shallow landslides showed signs of reactivation in the Darfield earthquake. Landowners north of the field area reported tension cracks in the weeks after the main shock, but these were predominantly found around pre-existing features, typically in shallow, scalloped soil slides, and finite displacement could not be attributed solely to the Darfield earthquake. Aerial photographs of ‘fresh’ cracks days after the quake indicate that motion was recent. Ground reconnaissance of ~20 m long, ridge-parallel cracks in this area showed that they occurred at the head scarps of pre-existing landslides. There was no vertical component observed in these cracks, and extension was small (5–10 cm) compared to the other ridge-parallel cracks described in this study. The features were mapped and logged but not considered as continuations of the features on the southern end of the Harper Hills. Shallow landslides within the field area (Fig. 3) were not reactivated.

Pre-existing deep-seated landslides were mapped using aerial photography and a 15 m DEM. The prominent ridge line scarp to the NE of the modern cracks was mapped by Muirson (2003) and an extensional depression in the central portion of the field area was identified in this study (Fig. 3).

4. Subsurface investigation of the Harper Hills landslide

4.1. Trench investigation

A 2.5 m deep by 4 m long trench was excavated across a prominent ground crack in the zone of the highest crack displacements and fissure depths (Figs. 4B and 7). Following excavation, the walls and a section of floor were scraped clean of excess material left by the backhoe. Due to the rapid desiccation of the excavated material and resultant change in observable soil properties, one of the walls (North Wall, Fig. 7) was chosen for detailed cleaning and the other was allowed to weather for three days. Both walls and a section of floor were gridded at 1 m horizontal and 0.5 m vertical intervals (0.5 m NE and 1 m SE for the floor). Photographs of each grid section were taken and corrected for any distortion from the camera angle. Logging was then conducted directly onto the corrected orthophotos.

The North Wall of the trench reveals the modern slip plane that propagates to the surface and vertically displaces the soil profile. On the up-thrown block of this structure, subsidiary shears with normal displacement are oriented at ~60° to the main trace. These features were observed at the surface immediately after the rupture (fissure orientation in Fig. 4C) but have subsequently degraded and become subdued. There is a forward rotation of 9° within 75 cm up-slope of the slip plane. At the base of the scarp free face, small amounts of mineralized A-horizon and sandy material from the exposed E-horizon have accumulated. A fissure on the up-dip extension of the slip plane has been in-filled with this material, though it is unclear if this fissure is coseismic or related to the shrink-swell (and subsequent in-fill) nature of the soil, for which there is pedogenic evidence in the veins of the underlying fragipan.

The downthrown block contains a broader zone of deformation (~1 m) than the up-thrown block, which is commonly observed in trenches across normal faults (McCalpin, 1987). There is a small component of backtilt (5°) upslope due to the SE-dipping, listric geometry of the slip plane in the shallow subsurface. This plane cannot be traced into the floor, which implies that its geometry is controlled by the soil stratigraphy at the surface (i.e. does not rupture through harder material, see below). The rotation is therefore superficial at the ground surface and not related to overall landslide kinematics. Measurements of vertical surface displacement using the far-field slope match those observed in the soil profile at depth.

Downslope of the slip plane, deformation is marked by an A-horizon that has washed down into vertical fissures. Beneath 18 cm (down from the surface), leached A-horizon material can be found coating narrow, closely spaced cracks. These cracks form naturally in the Bt, Bt2, and

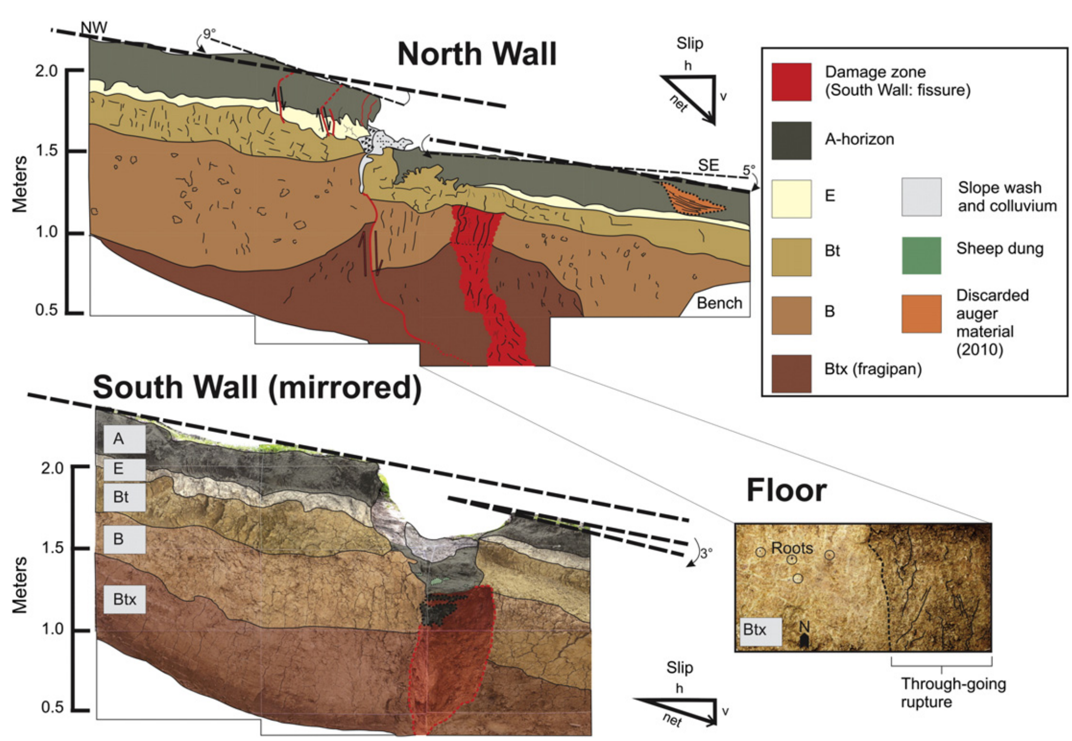

Fig. 7. Landslide trench. Trench across the head scarp of the Harper Hills landslide. The South Wall is shown with transparent units to show the soil structure of the weathered face. Rotations are indicated by dashed lines on the ground surface and arrows. Slip triangles are derived from the vertical displacement (v) and extension (h) across the deformation zones. The width of the damage zone on the North Wall is considered as the amount of extension, though not expressed at the surface. See Table 1 and text for discussion.

Btx horizons (South Wall, see below), but are particularly dense and wider in the 1 m zone downslope of the scarp. A 30 cm-wide zone of loose B-horizons and leached A-horizon occurs on the downslope extremity of the deformed zone. While this 'damage' zone does not break the base of the A-horizon, it is developed in the basal fragipan and joins the main slip zone on the South Wall (annotated photo of trench floor in Fig. 7). It is interpreted to represent an along-strike die out of the extension on the South Wall (below), as there is no evidence to suggest it is a previously filled fissure. The scarp-forming slip plane cannot be traced down-dip to the bottom of the trench.

The South Wall, which was allowed to dry and weather, displays the soil stratigraphy more clearly (transparent units, Fig. 7). A strong, basal fragipan is the most defined horizon and limited the depth to which the trench could be excavated. It is impermeable at its base where water can be seen accumulating. Floor exposures show that it consists of heavily oxidized polygons of loamy fine sand, with clay content increasing downward, rare basalt pebbles (<5%) and grey silt veins (yellow-grey soils of Raeside, 1964; Gradwell, 1974). Woody roots (~2 cm diameter) penetrate the softer, permeable silt veins on the trench floor, and are likely remnants of a pre-human, low land to montane, conifer–broadleaf forest that spanned the Canterbury plains (Molloy et al., 1963; McGlone, 1989). Deforestation in this region took place primarily from about 750 to 500 years BP due to anthropogenic burning, although climate induced forest reductions occurred from about 3000 years BP (McGlone, 1989; McGlone and Wilmshurst, 1999). By the time of European surveys c. 1840 CE, most, if not all, of the Canterbury plains was deforested (McGlone, 1989). The silt veins in the fragipan developed before the roots exploited them as zones of weakness. The minimum age of the fragipan is thus likely to be older than 500–750 years BP, and probably older than about 3000 years BP (see below for discussion).

The scarp morphology on the South Wall is markedly different. Greenish-blue pockets of sheep dung beneath what appears to be down-dropped A-horizon indicates that not all of the fissure sedimentation is natural. Below the ovinogenic layer (34 cm below the surface), however, a block of modern A-horizon has been preserved within the Bt-horizon. This block was exposed when a ~35–50 cm-wide, unconsolidated area in the fracture zone collapsed from the trench wall, a width which generally agrees with crack measurements in this location immediately post-quake (30 cm extension). There is a small component of forward (down-slope) rotation on the down-thrown block of 3°.

The net slip vectors for each wall were drawn using several measurements of extension and vertical displacement (Fig. 7). Variations in the soil thickness and gradational contacts contribute to error which we estimate as ± 10 cm. While the individual components on each wall vary significantly, the net slip vectors (0.46 and 0.54 m for the North and South Walls, respectively, assuming the damage zone width on the North Wall is analogous to extension on the South Wall) are comparable and match measurements taken at the surface after the event (0.50 m).

4.2. Ground penetrating radar (GPR)

A 90 m GPR survey was conducted across the major set of cracks in an attempt to map the subsurface geometry of identified surface fractures and to identify any unrecognized subsidiary features. The imaging was done using a Sensors & Software pulsEKKO system, with both 100 and 50 MHz antennas. The antennae were mounted on a sled, and towed from the lower GPS reference point to a point over the crest of the hill, and the profile was repeated by towing the sled back down to the reference point. This was done to test repeatability and to yield a number of profiles from which we could choose the one with the least amount of noise. Noisy traces can cause anomalous features in the processed data, particularly in migrating the profiles.

Markers were placed on the ground at regular intervals and as each marker was passed, a marker was placed on the file. These *fiducial markers* were then used to interpolate the continuously acquired traces to yield profiles with equally spaced traces. The sled was towed slowly so that the number of traces acquired far exceeded the number of traces needed for optimum resolution of subsurface features. The average trace spacing was less than 10 cm for the 100 MHz antennas, and less than 50 cm for the 50 MHz antennas. The interpolated trace spacing used for the 100 MHz profiles was set to 10 cm, or 10 traces per meter, and the spacing used for the 80 MHz profiles was set to 50 cm, or 2 traces per meter.

Diffractions in the unprocessed dataset are the result of scattering from features such as rocks, roots, and truncations of bedding. The curvature of the diffraction hyperbolae are inversely related to the square of the subsurface radar velocity. The "best fit" velocity was determined to be 80 m μs^{-1} (0.08 m ns^{-1}). This is typical for a moist but not saturated fine-grained soil. The depths estimated by converting the travel times to depth were checked against the depths of the soil layers in the trench, in particular the fragipan that appears to have been the deepest reflective boundary at this site. The "best fit" velocity in this case appears to be about 100 m μs^{-1} (0.10 m ns^{-1}). This discrepancy may be due to the fact that the diffractions are originating from shallower subsurface features and the deeper velocity is faster.

The 80 m μs^{-1} velocity was used to migrate the profiles. The process of migration collapses the diffractions to points, and places dipping features into their correct geometric positions. If too-high a velocity is used, then the diffractions are turned inside out and become "smiles" (noise spikes also become smiles regardless of the migration velocity used). The resultant migrated profiles, with topography added, are shown in Fig. 8. The profiles have been converted to elevation using the 100 m μs^{-1} velocity so that the depth to the fragipan is more realistic. The fragipan is demarcated by dashed lines at 2–2.5 m depth in both profiles.

The modern deformation zone occurs at 50–60 m distance in both profiles (Fig. 8). In the 100 MHz profile (Fig. 8A), there is clear offset of two blocks on three structures, one of which at 55 m was observed in the trench and reaches the surface. The vertical offset of the reflectors on this structure is 27–30 cm, which is comparable to vertical offset measured on the North Wall of the trench (29 cm). The other two structures are inferred from offset or folded reflectors, but do not reach the surface. The structures are sub-vertical and appear to dip more shallowly into the slope beneath the fragipan, but the penetration of the 100 MHz antennae drops off near this depth making interpretation difficult. Directly downslope of the three structures, the reflectors appear to be drag folded, consistent with normal motion at the head scarp. From 30–45 m in the 100 MHz profile, there is expression of a possible graben or rotational wedge in the subsurface. While it is uncertain what the kinematics of the two bounding structures are, they are clearly oppositely dipping and occur at slope inflection points at the ground surface.

The 50 MHz profile (Fig. 8B) has less resolution but a greater depth of penetration, allowing for alternative and/or supplementary interpretations of the near surface kinematics. The head scarp geometry is less clear than the 100 MHz profile but similarly suggests offset on vertical to near-vertical structures. The deformation zone at 30–45 m along the profile is better imaged by the 50 MHz antennae and concave reflectors suggest it is more likely to be a graben. At 3–4 m depth, a discontinuous, 'noisy' reflector is likely to be the top of the Harper Hills Basalt. Displacement and rotation on structures dipping into the slope between 0 and 30 m imply that joints in the Harper Hills Basalt accommodate some of the slope failure. It is unknown whether this deformation was pre-existing or occurred simultaneously with head scarp motion in the Darfield earthquake.

5. Discussion

5.1. Landslide kinematics

The consistent crack extension direction and horizontal extension indicate primarily translational kinematics. Near the south-western extent of the cracks, tension oriented ~45° to the predominant direction of

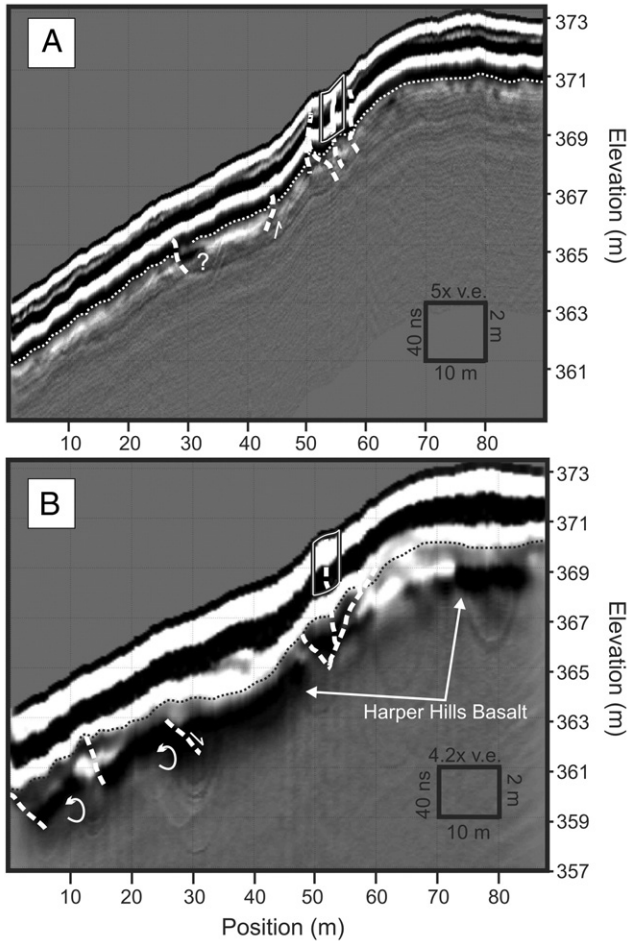

Fig. 8. GPR Profiles from the 100 MHz (A) and 50 MHz (B) ground penetrating radar (GPR) surveys across the trench site. Utilizing two frequencies allows for alternative and/or supplementary interpretations of landslide geometries. The fragipan is a strong reflector and its base is demarcated by a thin dashed white (100 MHz) or black (50 MHz) line. Trench locations are outlined in solid white lines outlined black. Slip surfaces are dashed where inferred and solid where definite. Trench stratigraphy and displacement match well with observations from the 100 MHz profile, and both profiles show evidence for deformation down-slope of the head scarp.

motion is the inferred surface manifestation of incipient strike-slip shear on the flank of a coherent spread or translational slide (Technical Advisory Group, 1991; Muller and Martel, 2000). The remediated crack 460 m down-slope of the head scarp and features observed in the GPR are also indicative of internal deformation of a coherent, translational landslide.

The landslide is considered to be deep-seated (>3 m depth, well below rooting depth), as a subsurface 'damage' zone was observed to rupture a dense fragipan in the trench at ~2.5 m depth. The GPR profiles show structures penetrating to at least 3–4 m depth. At the surface, cracks can be traced cutting across topography (Fig. 4A) while running parallel to strike of the Harper Hills bedrock geology, which lends itself to down-dip, rather than simple down-slope motion. Fig. 6 shows that crack extension direction is most coincident with bedding dip-direction. Pre-existing shallow landslides showed only minor motion compared to displacement on the main cracks, also pointing towards failure driven by bedding plane weaknesses. It is possible that slip on the Chalk Hill Clay could have facilitated down-dip translation as has been inferred for more discrete ridge-line failures NE along the Harper Hills. The 21° residual internal friction angle of the unit is significantly less than the slopes where the failures occurred (Muirson, 2003).

Down-dip projection of bedding from a contact between Harper Hills Basalt and Sandpit Tuff observed in Fig. 6 coincides with a bulge at the base of the Harper Hills which could be a toe of a pre-existing failure (Fig. 9A). The intense brecciation of the Sandpit Tuff (Browne, 1983), and its variable thickness overlying the Chalk Hill Clay, make both units possible slip surfaces for the Harper Hills landslide. If it is the basal failure plane, the volume involved in total failure of the slope is a maximum of 6.9×10^7 m^3.

Where observed, rotation appears to be caused by slumping from scarp degradation and secondary (i.e. superficial) fracturing. The down-dip tapering, listric slip plane on the North Wall of the trench accounts for a small component of up-slope backtilting, though this backtilt was not observed elsewhere. Down-slope rotation of the down-thrown block at places, as implied by fissures that narrow with depth and observed in the 50 MHz GPR profile, may be due to translation accompanied by toppling on joint-bounded basalt blocks (Figs. 8 and 9B). The mode of failure illustrated in Fig. 9C fits well with our observations of crack morphology and structural geology, and matches observations of earthquake-induced ridge spreading and fissuring elsewhere (Agliardi et al., 2001; McCalpin and Hart, 2002; Sleep, 2011; Gutiérrez et al., 2012). The features observed in this study probably fall on a continuum between coherent landslide and ridge-top spreading, as proposed by McCalpin and Hart (2002).

Both crack displacement and depth increase with decreasing ridge-to-crack relief (Fig. 5). This could be an effect of topographic and geometric amplification, which allows for maximum ground displacement at ridge crests and decreases quickly away from these areas (Meunier et al., 2008; Buech et al., 2010). If indeed due to topographic amplification, this observation also lends itself to a component of joint-controlled toppling at the head scarp: deeper cracks with more extension occurred nearest the top of the ridge. There is no clear reason for bedding-controlled translation to respond to amplification by producing the crack depth/displacement gradient observed. However, without further controls on variations in soil properties along the ridge, we cannot state conclusively that this pattern is solely a result of topographic or geometric amplification.

In contrast to the deep-seated landslide studied by Muirson (2003), which had surface movement rates of 24 cm year^{-1} during 2002–2003, no detectable motion was observed on the Harper Hills landslide in 2 years of surface monitoring. Post-quake measurements and subsurface crack widths in the trench confirm this observation. Without further constraints on stratigraphic and water table differences between the current study area and that of Muirson (2003), we are unable to speculate on future, creeping motion of the Harper Hills landslide. However, there is some evidence that progressive displacement has not been occurring in the last thousand years. Trenching and GPR did not reveal conclusive evidence for previous head scarp displacement, though features in the GPR could have formed in past events. Roots post-dating fragipan development at the base of the trench are probably a minimum of 500–3000 years old, but have not been dated (McGlone, 1989; McGlone and Wilmshurst, 1999; McWethy et al., 2009). In the Eastern USA, Ciolkosz et al. (1992) postulated a period of 6–18 ka for fragipans to develop, and 'proto-fragipans' have developed within 4500 years in Pennsylvania (Cremeens et al., 1998; Ciolkosz and Waltman, 2000). Age constraints on fragipan genesis elsewhere are tenuous, but there are indications that it takes several thousand years (Bockheim and Hartemink, 2013). If age ranges from the USA are adopted in this study, the age of the soil could be as old as 6.75–21 ka. A progressively deforming slide moving at 24 cm year^{-1}, or even a tenth of this rate, would have moved up to several kilometers in that time. There is no evidence for this amount of material being transported in the field area, though a pre-earthquake toe bulge near the base of the slope (Figs. 3 and 9) that is present in pre-quake digital elevation models could indicate at least some down-slope creep. Mountjoy and Pettinga (2006) note that deep-seated landslides in Tertiary soft-rock terrain of New Zealand are predominantly controlled by periodic earthquake

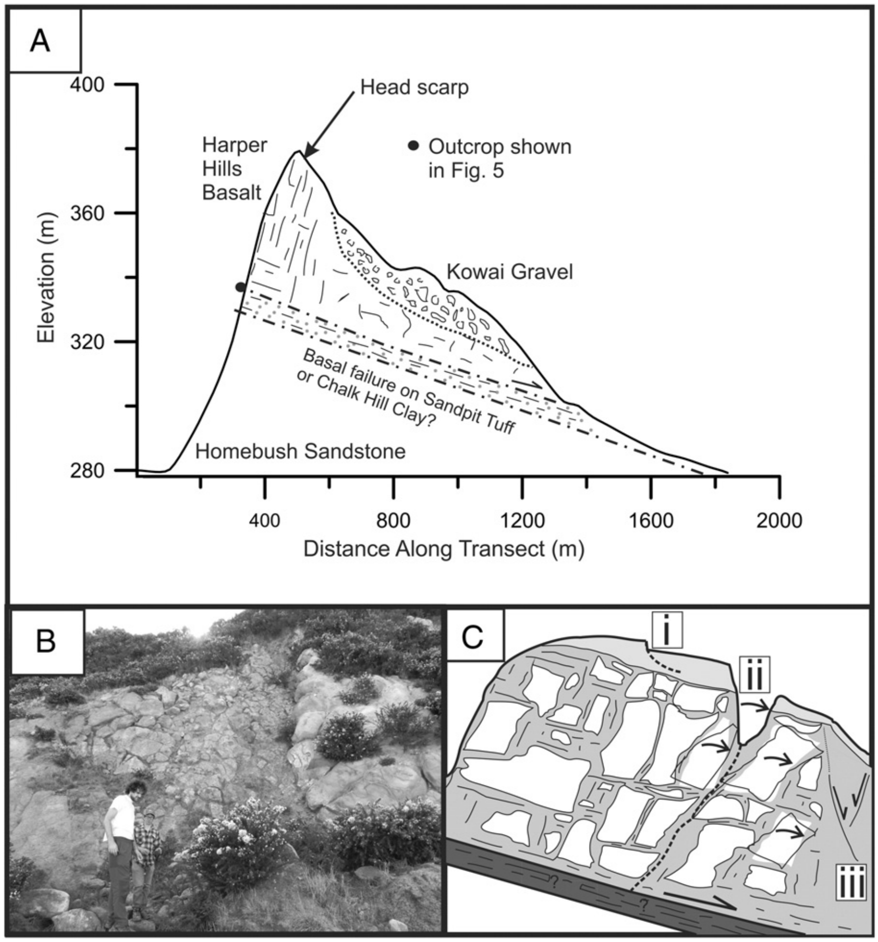

Fig. 9. Cross-section and failure mechanism. A) Schematic cross section of the Harper Hills landslide with bedding-plane failure in the Sandpit Tuff/Chalk Hill Clay. B) Heavily jointed and brecciated basalt along the Harper Hills ridgeline NE of the field area. C) Proposed failure mechanism of combined bedding-plane translation and joint-controlled toppling leading to extension and vertical displacement: (i) Shallow (i.e. superficial) listric slip in soil due to broad extension at head scarp and mechanical differences of soil horizons (as in trench); (ii) Ground cracking and fissuring with both vertical displacement and horizontal extension; and (iii) Internal deformation of coherent slide, not always rupturing the surface (as in trench/GPR).

shaking, though catastrophic failure can occur well after initial motion (e.g. Pettinga, 1987).

5.2. Paleoseismology

New Zealand's national seismic hazard model predicts a 1–2.5 ka return period for peak horizontal accelerations (0.45–0.51 g) that the Harper Hills experienced in the Darfield earthquake (for Class C shallow soils) (Stirling et al., 2008; Cousins and McVerry, 2010; Stirling et al., 2012). A critical acceleration for landslide initiation is difficult to constrain as subsequent aftershocks that did not generate any clear surface manifestations of landslide movement only generated PGAs of <0.1 g at the study site (Table 2). Rigid-block, coupled and decoupled Newmark analyses using SLAMMER software (Jibson, 2011; Jibson et al., 2013) indicate that the net displacements we measured of 22 and 55 cm (average and maximum, respectively) and acceleration-time history are consistent with critical accelerations of 0.1–0.16 g for the Harper Hills landslide (Table 3). If Newmark displacements are indicative of field displacements (e.g. Pradel et al., 2005), then smaller episodic displacements should be expected at return periods of less than 150 years (Stirling et al., 2001). However, the likelihood of internal deformation within the Harper Hills landslide and the inability of Newmark analyses

Table 1
Trench unit descriptions.

Unit/horizon	Color (moist)	Texture	Structure	Notes
A	7.5YR 2.5/1	Silt loam		Transitional into E-horizon
E	7.5YR 7/2	Silt loam	Granular	Mottled, bioturbated lower boundary
Bt	2.5Y 4/3	Clay with some silt; silt and sand content increasing towards base	Massive to blocky	Desiccation cracks abundant: dipping subvertically to steeply up-hill
B	2.5Y 5/3	Sandy clay loam w/dark vesicular basalt lithics	Blocky to prismatic	Basalt sapprolite pebbles present (~5%)
Btx	2.5Y 5/4; 5Y 6/2 (veins)	Loamy fine sand to silt Fine silt (veins)	Gammate	Desiccation cracks narrowing into basal, dense fragipan marked by increase of clay coating sand grains; rare basalt pebbles
Damage zone	2.5Y 5/3–4	–	Massive, indistinct	Soil boundaries obscured across zone; low cohesion; modern roots grow preferentially in zone; leached A-horizon infilling and coating cracks

Table 2
Strong ground motions recorded at HORC for main shock and aftershocks.

Date (UTC)	Time	M_W	PGA_h (g)	PGA_v	Epicentral distance to HORC (km)
3 Sep. 2010	16:35:46	7.1	0.45	0.79	20
4 Sep. 2010	4:55:56	4.7	0.05	0.04	1.9
4 Sep. 2010	8:54:27	4.1	0.03	0.02	6.3
5 Sep. 2010	16:06:26	4.5	0.02	0.01	9
6 Sep. 2010	11:40:50	4.8	0.07	0.08	8.3
6 Sep 2010	15:24:44	5.4	0.01	0.009	26

to suitably model dynamic sliding conditions make interpretations of predicted return periods at the site difficult. Rather, if PGAs in the main event are indicative of the required shaking for failure, episodic displacement would be expected on 1–2.5 ka timescales at the Harper Hills.

Although there are no absolute age data on the soil in the current study, it is probable that the fragipan (Btx) developed over thousands of years (see above). Since trenching did not reveal any prior events over a time period greater than the predicted return period of strong ground motions at the site, one or a combination of the following must be true: a) past events of similar PGAs were not preserved or did not induce cracking at the trench site, b) PGAs are not the only seismologic factor in determining landslide initiation, and/or c) PGAs equal to or above the landslide-triggering threshold have not occurred at the study site over the time interval captured within the trench record. While (c), the underestimation of return periods for a given ground motion in PSHAs, has been studied in some detail by Brune (1999) and Brune et al. (2006), we focus our discussion on (a) and (b) below.

5.2.1. Head scarp and subsurface preservation

The ability to recognize evidence for past landslide events depends on the preservation of head scarp features in the subsurface as well as trench location. Whether or not the modern head scarp has been repeatedly reactivated in the past may be difficult to constrain. Vegetation may have stabilized the shallow subsurface in previous events and thereby reduced the susceptibility of the ground surface to the type of discrete cracking observed within the contemporary agricultural landscape. GPR did not show conclusive evidence for pre-existing deformation within 45 m up and downslope of the modern cracks, though further trenching and dating would have to be conducted to further investigate this. Modern deformation does not necessarily pierce the surface, as has been observed in the trench (North Wall 'damage' zone, Fig. 7). Thus, offsets observed in the GPR profiles are small enough (i.e. comparable to direct measurements made in the trench) to be considered to have occurred only in the most recent event.

Increasing crack displacement and depth with proximity to the ridge suggests that the trench location chosen was ideal for identification of older features, although it is unclear if this pattern would have been repeated by past events. Evidence from trenches in ridge-top spreads and sackungen elsewhere in the world suggest that it is more common for episodic displacement to occur at the same location on a scarp or ground crack than elsewhere if the displacement is greater than 3–5 cm horizontal and 1–3 cm vertical (Technical Advisory Group, 1991; Nolan and Weber, 1992, 1998; McCalpin and Hart, 2002). The displacement at the trench site well exceeded these values, but this relationship may change due to spatial and temporal changes in the soil mechanical properties.

The preservation and recognition of prior events in a trench depend on the scarp morphology, soil stratigraphy and offset. In this study, scarp morphology and the amount of offset determine the accommodation space, and thus volume of material available for syn- and post-event deposition. Graben or fissures (Fig. 10A–C) create the most space and have the highest preservation potential, whereas cracks with primarily vertical displacement have less space and rely on the erosion of a free face.

Secondary slumping and shearing of the A and E horizons observed on the North Wall of the trench would go unnoticed without a surrounding B horizon for contrast (lower A-horizon block on the South Wall). With further soil development, the only remnant of vertical cracks will be a slightly thickened A-horizon on the down-thrown block. Even with sufficient burial, preservation of a discrete, organic soil block over >1000 ka is tenuous and evidence for past events would 'anneal'. A-horizon film coating cracks on both walls is not likely to persist over hundreds of years and could form by desiccation just as easily as by landslide induced tension.

The best opportunity for preservation and recognition of older features is via fissure-fill style deposition. Observations of crack degradation from 2 months to 2 years after the Darfield earthquake, though subject to human and sheep modification, show that this deposition takes place on features with the greatest component of extension (Fig. 10A–C). Interpretations of smaller fissure-like features in this study are complicated by the shrink-swell nature of the B-horizons.

Observations of ground cracks following the Loma Prieta earthquake and this study show that cracks and fissures are vertically discontinuous up and down-dip (Technical Advisory Group, 1991). For example, the subsurface, extensional 'damage' zone (Table 1, North Wall in Fig. 7) coincides with surface rupture on only one of the two walls, and the primary slip plane on the North Wall cannot be traced onto the floor exposure. This implies that over a 2 m scale, the characteristics of fissuring and displacement on discrete structures can change drastically. In the 50 MHz GPR profile, deformation in the underlying Harper Hills Basalt does not always have a surface expression. Up-dip propagation to the surface of structures within the slide body may occur over several episodes, or not at all. Extension from older events may not have ruptured the surface, and, depending on stratigraphy, may not show identifiable offset in the subsurface. It is advisable to log all faces of the trench, when possible, to decrease the possibility of false negatives and develop a full model of kinematics at the surface.

5.2.2. Peak ground acceleration and other factors

Slope response during an earthquake relies on a number of factors. Peak horizontal acceleration and shaking duration, widely used in Newmark displacement analyses, are only two seismic parameters that will influence landslide-triggering (Jibson and Keefer, 1993; Jibson, 1996). The effect of vertical accelerations could play a major role in reducing shear strength in detachment horizons, particularly for near-source, deep-seated landslides (Huang et al., 2001; Ingles et al., 2006). Slope orientation and topography can increase susceptibility by redistributing wave energy into slope-normal components (Del Gaudio and Wasowski, 2007) and rupture-sourced forward directivity affects the occurrence of landslides (Jibson et al., 2004; Sleep, 2011).

Table 3
Newmark analysis parameters and output. [1] HORC N00E component (PGA direction) input acceleration-time history; [2] Landslide thickness of 30 m; Shear wave velocities of units above and below failure plane derived from Bienawski (1989), Carlson et al. (1980), Kowallis et al. (1984), and Muirson (2003): Harper Hills Basalt = 3900 m/s; Homebush Sandstone = 1500 m/s; Damping ratio of 5% and reference strain of 0.05% (Jibson et al., 2013). Critical accelerations were calculated iteratively by optimizing to the range of Newmark displacements to match field displacements.

Model	Input parameters	Newmark displacement$_{avg}$ (cm)	Field disp.$_{avg}$ (cm)	Ac$_{avg}$ (cm)	Newmark displacement$_{max}$ (cm)	Field disp.$_{max}$ (cm)	Ac$_{max}$ (cm)
Rigid-block	[1]	21.81	22.2	0.16	53.16	54.6	0.1
Decoupled	[1], [2]	21.37			51.54		
Coupled	[1], [2]	24.45			55.29		

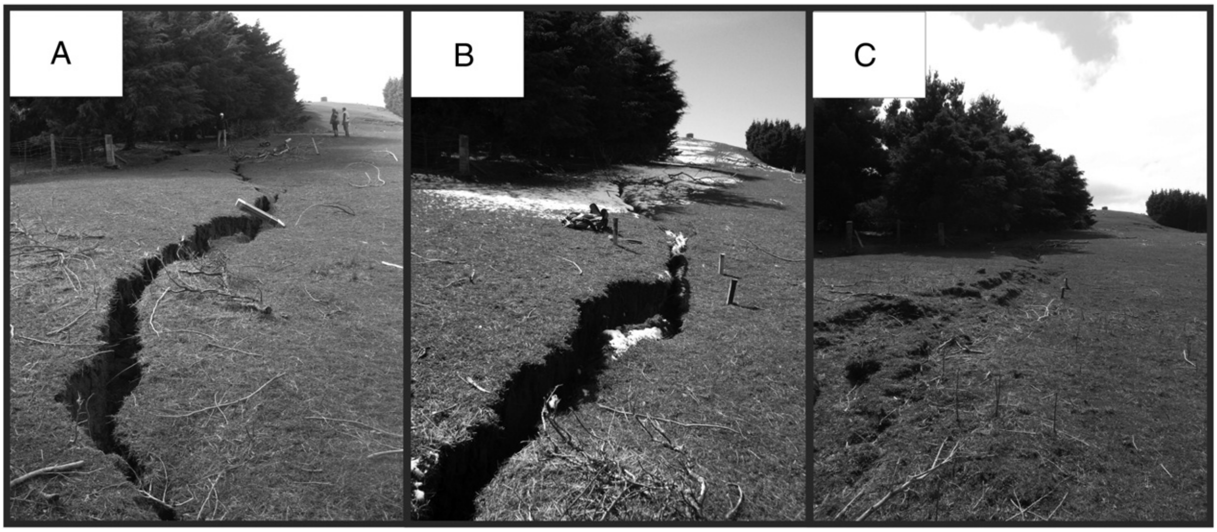

Fig. 10. Preservation potential of the head scarp. Harper Hills scarp degradation and fissure-fill through time. A) Two days after the quake. B) Two months after the quake. C) Two years after the quake, probably altered by anthropogenesis and ovinogenesis, but showing the style of deposition likely to occur if left over longer time periods.

Darfield earthquake ground motions recorded near the Harper Hills principally reflect rupture of the HAF and the western Greendale Fault (Fig. 1). The main ground cracks observed in this study are discontinuous north-eastward across the sub-surface Greendale Fault. High accelerations starting at ~20 s into the earthquake sequence at HORC and spanning the 5–95% significant duration of 8.7 s correlate with rupture of the HAF (Holden et al., 2011; Bradley, 2012). Vertical PGAs at HORC were more than double those of the nearest station on the NE side of the Greendale Fault, probably due to near-source effects that enhanced ground motion (Abrahamson and Somerville, 1996; McVerry et al., 2006; Meunier et al., 2007; Bradley, 2012) and close proximity to the HAF. Velocity pulses in both the E–W and N–S components at HORC are indicative of forward directivity of the bilaterally rupturing Greendale Fault and HAF (Bradley, 2012).

While no attempt is made here to model the complicating effect of these ground motion characteristics on slope failures in the Harper Hills, it is suggested that they offer insights into the lack of prior fissures observed in the trench. Hanging-wall amplification and forward directivity are linked to the specific rupture kinematics in any given earthquake, and can thus be expected to have longer return periods than modelled horizontal PGAs. A lack of evidence for prior events in our trench could indicate that ridge failure on the Harper Hills landslide is associated with a site response resulting from Darfield earthquake-type fault kinematics and source characteristics (Fig. 11). For ground cracks generated in the Loma Prieta earthquake, Nolan and Weber (1998) concluded that cracks may only form in specific, multi-segment events on the San Andreas Fault based on a longer return period of crack displacement than faulting. Preliminary analyses indicate that the

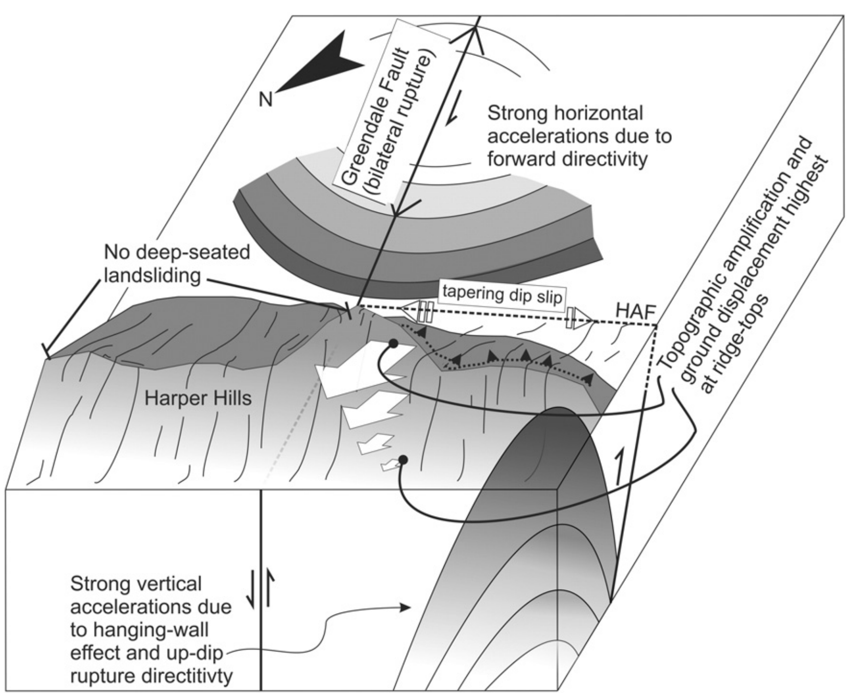

Fig. 11. Influences on landslide failure and location. Block model of the Harper Hills, with topographic and seismic-source effects on the occurrence of deep-seated landsliding. Ground cracks were only observed on the hanging wall of the Hororata Anticline Fault (HAF) and Greendale Fault, the former being truncated by the subsurface Greendale Fault. It is proposed that rupture directivity affects the location of cracks, and that crack location and displacement (e.g. Fig. 5) may be related to topographic amplification of incoming seismic waves.

penultimate earthquake on the Greendale Fault occurred between ca. 22 and 28 ka (Hornblow et al., unpublished results); if the specific seismologic characteristics of earthquakes resulting from this fault rupture have a first order control on the location of the landslide head scarp documented in this study, then a similarly long return time of landslide reactivation at the trench site might be expected.

5.3. Implications for future studies

Ridge-top ground cracks, sackung, and large translational slides have been reported in several historical earthquakes (c.f. Technical Advisory Group, 1991; McCalpin and Hart, 2002; Gutiérrez et al., 2008). There have been comparatively few trenching studies of documented co-seismic landslide scarps and/or fissures, though most trenches have revealed evidence for prior events (Technical Advisory Group, 1991; Nolan and Weber, 1992, 1998; McCalpin, 1999). The key questions in paleoseismic investigations of these scarps are a) Is motion episodic or progressive? b) If prior episodic displacement is observed in the trench, can a seismic origin be deduced? c) Is rupture of a specific fault or set of faults responsible for the observed displacement? Having constrained parts of these in the present study, we consider contributions to these questions below.

5.3.1. Episodic vs. progressive deformation

Trench location may assist in determining how a landslide fails. While the ground cracks in this study were undoubtedly formed in the Darfield earthquake, there are indications of on-going deep-seated landsliding down-slope of the modern cracks and along the Harper Hills ridge. We cannot, therefore, rule out an on-going interaction between progressive failure and episodic displacement caused by earthquake shaking. While it is clear that both triggering mechanisms occur in nature, paleoseismic trenches typically produce evidence of only one mechanism. When both are observed, colluvial deposition on the down-thrown block will either produce cumulic soil horizons (progressive deformation) or buried soils (episodic) (Technical Advisory Group, 1991). Patterns of folding and offset in well stratified material can also reveal a history of motion (e.g. McCalpin et al., 2011). In the current study, it is unlikely that a distinction could be made between the two soil types for scarps without a component of extension because the soil stratigraphy is relatively homogeneous. Fissures with large amounts of extension are more likely to form episodically and fissure stratigraphy will indicate more clearly if opening occurred abruptly or over time (Fig. 10). Therefore, if the geomorphology is suggestive of graben or fissure development, these areas should be targeted for trenching studies over scarps with vertical displacement alone.

5.3.2. Seismic vs. aseismic origin

Deep-seated translational landslides can be caused by earthquake shaking, raised water tables (Johnson and Cotton, 2005), glacial debuttressing and/or fluvial undercutting (Gutiérrez et al., 2008). Determining a seismic origin of episodic displacement can be difficult and relies on independent age control of primary tectonic features and corroborative age control on other landslide features (McCalpin and Hart, 2002; Gutiérrez et al., 2008). From our observations, a seismic origin can be considered if head scarp displacement and depth covary with site effects that amplify incoming waves (Fig. 5). For example, if several trenches reveal a pattern whereby age-correlated fissures closer to the ridge or overlying weaker soil have the greatest displacement, it is possible that they formed co-seismically. This conclusion matches our results, but more field studies and numerical modelling should be carried out to test this hypothesis, as similar displacement profiles might be created from other triggers.

5.3.3. Relationship to specific (paleoseismic) faulting events

Establishing a relationship of landslide displacement with specific or recurrent earthquakes requires a long record of sympathetic, tightly age-bracketed events (McCalpin, 1999; McCalpin and Hart, 2002). Slope stability modelling that includes different rupture scenarios, pore pressures, topographic amplification, forward directivity and vertical accelerations should be conducted to determine that the proposed fault system can induce failure. In regions where faulting is blind, or obscured by geomorphic processes, these parameters may be impossible to determine. Difficulties in determining a history of multi-fault ruptures and longer term, static-stress triggered seismicity, as well as in event recognition and preservation, further complicate the use of landslides as secondary paleoseismic evidence. This is not to say that seismic origins of landslides cannot be deduced, or that landslides in regions with historical seismicity and limited seismic sources cannot be linked to earthquakes on a given fault system using Newmark analyses (e.g. Jibson and Keefer, 1993). However, in high seismicity regions like New Zealand, interpreting the seismic source from field data and without actual acceleration-time data is not advisable. The Darfield earthquake sequence may have led to 'characteristic ground-motions' (Brune, 1999; Brune et al., 2006) at the Harper Hills presenting the unique conditions for failure, even though the Darfield earthquake was allowed for in the New Zealand PSHA via a random, 'distributed' source model (Stirling et al., 2008). Unless there is an identifiable kinematic link between permanent deformation caused by faulting and ground failure, landslides in high seismicity regions are unlikely to yield useful information on specific fault sources.

6. Conclusions

Detailed geomorphic mapping, trenching, and GPR of the Harper Hills landslide have provided insights into its kinematics, failure mechanism, and paleoseismicity. The geomorphology and geology suggest predominantly bedding-controlled translation accompanied by inferred joint-controlled toppling at the head scarp. Measurements of crack displacement, depth, and position along slope indicate that shaking variability, possibly due to topographic amplification, is a factor in determining crack displacement. Trenching studies on similar features should concentrate on ridge-top graben or fissures for the best record of episodic displacements, and include several trenches to determine if there are indications of seismic triggering. Connecting evidence of strong ground motion in a trench to any one fault system requires considerations of complex fault rupture scenarios and resultant waveforms, site response characteristics, and preservation potential of the event in the stratigraphy. These factors present a difficult, but worth-while challenge for paleoseismologists seeking to derive a history of faulting at a site from landslide studies.

Acknowledgements

We would like to thank Rebecca Pannen, Richard Taylor, Sharon Hornblow, Brendan Duffy, Matt Cockcroft, Joshua Blackstock, Stefano, and Pilar Villamor for assistance in the field. John Beavan, Kevin Furlong, and Matthew Herman supplied useful InSAR and aftershock data. The Dennis family kindly allowed us to access to their farm for monitoring and trenching. We are grateful to James McCalpin and an anonymous reviewer for improving the quality of this manuscript. This research was funded by New Zealand Earthquake Commission (EQC) Capability Grant E5713 and a University of Canterbury International Doctoral Scholarship.

References

Abrahamson, N.A., Somerville, P.G., 1996. Effects of the hanging wall and footwall on ground motions recorded during the Northridge earthquake. Bull. Seismol. Soc. Am. 86 (1), S93–S99.

Agliardi, F., Crosta, G., Zanchi, A., 2001. Structural constraints on deep-seated slope deformation kinematics. Eng. Geol. 59 (1), 83–102.

Beavan, J., Samsonov, S., Motagh, M., Wallace, L., Ellis, S., Palmer, N., 2010. The Darfield (Canterbury) earthquake: geodetic observations and preliminary source model. Bull. N. Z. Soc. Earthq. Eng. 43, 228–235.

Beavan, J., Motagh, M., Fielding, E.J., Donnelly, N., Collett, D., 2012. Fault slip models of the 2010–2011 Canterbury, New Zealand, earthquakes from geodetic data and observations of postseismic ground deformation. N. Z. J. Geol. Geophys. 55, 207–221.

Bienawski, Z.T., 1989. Engineering Rock Mass Classifications: A Complete Manual for Engineers and Geologists in Mining, Civil, and Petroleum Engineering. Wiley-Interscience, Chichester, 272 pp.

Bockheim, J.G., Hartemink, A.E., 2013. Soils with fragipans in the USA. Catena 233–242.

Bradley, B.A., 2012. Strong ground motion characteristics observed in the 4 September 2010 Darfield, New Zealand earthquake. Soil Dyn. Earthq. Eng. 42, 32–46.

Browne, G.H., 1983. A new interpretation of brecciation in the Sandpit Tuff, Harper Hills, Canterbury. N. Z. J. Geol. Geophys. 26, 429–434.

Brune, J.N., 1999. Precarious rocks along the Mojave section of the San Andreas Fault: constraints on ground motions from great earthquakes. Seismol. Res. Lett. 70, 29–33.

Brune, J.N., Anooshehpoor, A., Purvance, M.D., Brune, R.J., 2006. Band of precariously balanced rocks between the Elsinore and San Jacinto, California, fault zones: constrains on ground motion for large earthquakes. Geology 34, 137–140.

Buech, F., Davies, T.R., Pettinga, J.R., 2010. The Little Red Hill seismic experimental study: topographic effects on ground motion at a bedrock-dominated mountain edifice. Bull. Seismol. Soc. Am. 100, 2219–2229.

Carbonel, D., Gutiérrez, F., Linares, R., Roqué, C., Zarroca, M., McCalpin, J., Guerrero, J., Rodríguez, V., 2013. Differentiating between gravitational and tectonic faults by means of geomorphological mapping, trenching and geophysical surveys. The case of the Zenzano Fault (Iberian Chain, N Spain). Geomorphology 189, 93–108.

Carlson, J.R., Grant-Mackie, J.A., Rodgers, K.A., 1980. Stratigraphy and sedimentology of the Coalgate area, Canterbury, New Zealand. N. Z. J. Geol. Geophys. 23, 179–192.

Ciolkosz, E.J., Waltman, W.J., 2000. Pennsylvania's fragipans. Pennsylvania State University Agronomy Series, 147 (12 pp.).

Ciolkosz, E.J., Waltman, W.J., Thurman, N.C., 1992. Fragipan in Pennsylvania soils. Pennsylvania State University Agronomy Series, 119 (14 pp.).

Cousins, J., McVerry, G.H., 2010. Overview of strong-motion data from the Darfield earthquake. Bulletin of the New Zealand Society for Earthquake Engineering 43 (4), 222–227.

Cremeens, D.L., Hart, J.P., Darmody, R.G., 1998. Complex pedostratigraphy of a terrace fragipan at the Memorial Park site, central Pennsylvania. Geoarchaeol. Int. J. 13, 339–359.

Del Gaudio, V., Wasowski, J., 2007. Directivity of slope dynamic response to seismic shaking. Geophys. Res. Lett. 34, L12301. http://dx.doi.org/10.1029/2007GL029842.

Duffy, B., Quigley, M., Barrell, D., Van Dissen, R., Stahl, T., Leprince, S., McInnes, C., Bilderback, E., 2013. Fault kinematics and surface deformation across a releasing bend during the 2010 M_w 7.1 Darfield, New Zealand, earthquake revealed by differential LiDAR and cadastral surveying. Geological Society of America. Geol. Soc. Am. Bull. 125, 420–431.

Elliott, J.R., Nissen, E.K., England, P.C., Jackson, J.A., Lamb, S., Li, Z., Oehlers, M., Parsons, B., 2012. Slip in the 2010–2011 Canterbury earthquakes, New Zealand. J. Geophys. Res. 117, B03401. http://dx.doi.org/10.1029/2011JB008868.

Forsyth, P.J., Barrell, D.J.A., Jongens, R., 2008. Geology of the Christchurch area. Institute of Geological and Nucelar Sciences 1:250000 geological map 16. 1 sheet + 67 pp.

Gledhill, K., Ristau, J., Reyners, M., Fry, B., Holden, C., 2011. The Darfield (Canterbury, New Zealand) Mw 7.1 earthquake of September 2010: a preliminary seismological report. Seismol. Res. Lett. 82, 378–386.

Gradwell, M.W., 1974. The available-water capacities of some southern and central zonal soils of New Zealand. N. Z. J. Agric. Res. 17, 465–478.

Gutiérrez, F., Ortuño, M., Lucha, P., Guerrero, J., Acosta, E., Coratza, P., Piacentini, D., Soldati, M., 2008. Late Quaternary episodic displacement on a sackung scarp in the central Spanish Pyrenees. Secondary paleoseismic evidence? Geodin. Acta 21, 187–202.

Gutiérrez, F., Lucha, P., Galve, J.P., 2010a. Reconstructing the geochronological evolution of large landslides by means of the trenching technique in the Yesa Reservoir (Spanish Pyrenees). Geomorphology 124, 124–136.

Gutiérrez, F., Soldati, M., Audemard, F., Bălteanu, D., 2010b. Recent advances in landslide investigation: issues and perspectives. Geomorphology 124, 95–101.

Gutiérrez, F., Linares, R., Roque, C., Zarroca, M., Rosell, J., Galve, J.P., Carbonel, D., 2012. Investigating gravitational grabens related to lateral spreading and evaporite dissolution subsidence by means of detailed mapping, trenching, and electrical resistivity tomography (Spanish Pyrenees). Lithosphere 4, 331–353.

Hart, M.W., Shaller, P.J., Farrand, G.T., 2012. When landslides are misinterpreted as faults: case studies from the western United States. Environ. Eng. Geosci. 18, 313–325.

Holden, C., Beavan, J., Fry, B., Reyners, M., Ristau, J., Van Dissen, R., Villamor, P., Quigley, M., 2011. Preliminary source model of the Mw 7.1 Darfield earthquake from geological, geodetic and seismic data. Proceedings of the Ninth Pacific Conference on Earthquake Engineering. Auckland, New Zealand, 8 pp.

Hornblow, S., Quigley, M.C., Nicol, A., Van Dissen, R.J., unpublished results, Paleoseismology of the 2010 Mw 7.1 Darfield (Canterbury) earthquake source, Greendale Fault, New Zealand.

Huang, C.C., Lee, Y.H., Liu, H.P., Keefer, D.K., Jibson, R.W., 2001. Influence of surface-normal ground acceleration on the initiation of the Jih-Feng-Erh-Shan landslide during the 1999 Chi-Chi, Taiwan, earthquake. Bull. Seismol. Soc. Am. 91, 953–958.

Ingles, J., Darrozes, J., Soula, J.C., 2006. Effects of the vertical component of ground shaking on earthquake-induced landslide displacements using generalized Newmark analysis. Eng. Geol. 86, 134–147.

Jibson, R.W., 1996. Use of landslides for paleoseismic analysis. Eng. Geol. 43, 291–323.

Jibson, R.W., 2011. Methods for assessing the stability of slopes during earthquakes—a retrospective. Eng. Geol. 122, 43–50.

Jibson, R.W., Keefer, D.K., 1993. Analysis of the seismic origin of landslides: examples from the New Madrid seismic zone. Geol. Soc. Am. Bull. 105, 521–536.

Jibson, R.W., Harp, E.L., Schulz, W., Keefer, D.K., 2004. Landslides triggered by the 2002 Denali Fault, Alaska, earthquake and the inferred nature of the strong shaking. Earthquake Spectra 20, 669–691.

Jibson, R.W., Rathje, E.M., Jibson, M.W., Lee, Y.W., 2013. SLAMMER—Seismic Landslide Movement Modeled using Earthquake Records: US Geological Survey Techniques and Methods 12-B1.

Johnson, P.L., Cotton, W.R., 2005. The Santiago landslide and associated ridge-top graben (sackungen): implications for paleoseismic landslide studies. Environ. Eng. Geosci. 11, 5–15.

Jongens, R., Barrell, D.J.A., Campbell, J.K., Pettinga, J.R., 2012. Faulting and folding beneath the Canterbury Plains identified prior to the 2010 emergence of the Greendale Fault. N. Z. J. Geol. Geophys. 55, 169–176.

Khajavi, N., Quigley, M., McColl, S.T., Rezanejad, A., 2012. Seismically induced boulder displacement in the Port Hills, New Zealand during the 2010 Darfield (Canterbury) earthquake. N. Z. J. Geol. Geophys. 55, 271–278.

Kowallis, B.J., Jones, L.E.A., Wang, H.F., 1984. Velocity–porosity–clay content systematics of poorly consolidated sandstones. J. Geophys. Res. 89, 10355–10364.

McCalpin, J., 1987. Recommended setback distances from active normal faults. Proceedings of the Symposium on Engineering Geology and Soils Engineering, 23 35–56.

McCalpin, J.P., 1999. Episodic earthquake-induced movement on the Stillwater scarp "sackung", central Nevada. Geol. Soc. Am. Abstr. Programs 31 (7).

McCalpin, J.P., Hart, E.W., 2002. Ridge-top spreading features and relationship to earthquakes, San Gabriel Mountains region. Southern California—Parts A & B. National Earthquake Hazards Reduction Program, USGS, Final Technical Report 51, 125 pp.

McCalpin, J.P., Irvine, J.R., 1995. Sackungen at the Aspen Highlands ski area, Pitkin County, Colorado. Environ. Eng. Geosci. 1, 277–290.

McCalpin, J.P., Bruhn, R.L., Pavlis, T.L., Gutierrez, F., Guerrero, J., Lucha, P., 2011. Antislope scarps, gravitational spreading, and tectonic faulting in the Western Yakutat microplate, south coastal Alaska. Geosphere 7, 1143–1158.

McGlone, M.S., 1989. The Polynesian settlement of New Zealand in relation to environmental and biotic changes. N. Z. J. Ecol. 12, 115–129 (Supplement).

McGlone, M.S., Wilmshurst, J.M., 1999. Dating initial Maori environmental impact in New Zealand. Quat. Int. 59, 5–16.

McVerry, G.H., Zhao, J.X., Abrahamson, N.A., Somerville, P.G., 2006. New Zealand acceleration response spectrum attenuation relations for crustal and subduction zone earthquakes. Bull. N. Z. Soc. Earthq. Eng. 39, 1–58.

McWethy, D.B., Whitlock, C., Wilmshurst, J.M., McGlone, M.S., Li, X., 2009. Rapid deforestation of South Island, New Zealand, by early Polynesian fires. The Holocene 19, 883–897.

Meunier, P., Hovius, N., Haines, A.J., 2007. Regional patterns of earthquake-triggered landslides and their relation to ground motion. Geophys. Res. Lett. 34, L20408. http://dx.doi.org/10.1029/2007GL031337.

Meunier, P., Hovius, N., Haines, J.A., 2008. Topographic site effects and the location of earthquake induced landslides. Earth Planet. Sci. Lett. 275, 221–232.

Molloy, B.P.J., Burrows, C.J., Cox, J.E., Johnston, J.A., Wardle, P., 1963. Distribution of subfossil forest remains, eastern South Island, New Zealand. N. Z. J. Bot. 1, 68–77.

Moro, M., Saroli, M., Gori, S., Falcucci, E., Galadini, F., Messina, P., 2012. The interaction between active normal faulting and large scale gravitational mass movements revealed by paleoseismological techniques: a case study from central Italy. Geomorphology 151 (152), 164–174.

Mountjoy, J., Pettinga, J., 2006. Controls on large deep-seated landslides in soft rock terrain: rock mass defects and seismic triggering. Proceedings of Technical Groups, New Zealand Geotechnical Society 2006 Symposium: Earthquakes and Urban Development, 31. Nelson, New Zealand, 10 pp.

Muirson, J.S., , 2003. An engineering geological investigation into slope movement at the Coalgate bentonite quarry, inland Canterbury. (MSc Thesis) Univ. Canterbury, New Zealand, 279 pp.

Muller, J.R., Martel, S.J., 2000. Numerical models of translational landslide rupture surface growth. Pure Appl. Geophys. 157, 1009–1038.

Nikonov, A.A., 1988. Reconstruction of the main parameters of old large earthquakes in Soviet Central Asia using the paleoseismogeological method. Tectonophysics 147, 297–312.

Nolan, J.M., Weber, G.E., 1992. Evaluation of surface cracking caused by the 1989 Loma Prieta earthquake, Santa Cruz County, California: case histories. In: Sharma, S. (Ed.), Proceedings of the 28th Symposium on Engineering Geology and Geotechnical Engineering. University of Idaho, Moscow, ID, pp. 272–286.

Nolan, J.M., Weber, G.E., 1998. Evaluation of coseismic ground cracking accompanying the earthquake: trenching studies and case histories in The Loma Prieta, California, earthquake of October 17, 1989—landslides. U. S. Geol. Surv. Prof. Pap. 1551-C, 145–163.

Onida, M., Galadini, F., Forcella, F., 2001. Application of paleoseismological techniques to the study of Late Pleistocene–Holocene deep-seated gravitational movements at the Mortirolo Pass (central Alps, Italy). Neth. J. Geosci. 80, 209–227.

Pettinga, J.R., 1987. Ponui landslide: a deep-seated wedge failure in Tertiary weak-rock flysch, Southern Hawke's Bay, New Zealand. N. Z. J. Geol. Geophys. 30, 415–430.

Pradel, D., Smith, P.M., Stewart, J.P., Raad, G., 2005. Case history of landslide movement during the Northridge earthquake. J. Geotech. Geoenviron. 131, 1360–1369.

Quigley, M., Villamor, P., Furlong, K., Beavan, J., Van Dissen, R., Litchfield, N., Stahl, T., Duffy, B., Bilderback, E., Noble, D., Barrell, D., Jongens, R., Cox, S., 2010. Previously unknown fault shakes New Zealand's South Island. EOS Trans. Am. Geophys. Union 91, 469–470.

Quigley, M., Noble, D., Van Dissen, R., Litchfield, N., Villamor, P., Duffy, B., Barrell, D., Furlong, K., Stahl, T., Bilderback, E., 2012. Surface rupture during the 2010 M_w 7.1 Darfield (Canterbury) earthquake: implications for fault rupture dynamics and seismic-hazard analysis. Geology 40, 55–58.

Raeside, J.D., 1964. Loess deposits of the South Island, New Zealand, and soils formed on them. N. Z. J. Geol. Geophys. 7, 811–838.

Sleep, N.H., 2011. Deep-seated downslope slip during strong seismic shaking. Geochem. Geophys. Geosyst. 12 (12), Q12001. http://dx.doi.org/10.1029/2011GC003838.

Stirling, M., Pettinga, J., Berryman, K., Yetton, M., 2001. Probabilistic seismic hazard assessment of the Canterbury region, New Zealand. Bull. N. Z. Soc. Earthq. Eng. 34, 318–333.

Stirling, M., Gerstenberger, M., Litchfield, N., McVerry, G., Smith, W., Pettinga, J., Barnes, P., 2008. Seismic hazard of the Canterbury Region, New Zealand: new earthquake source model and methodology. Bull. N. Z. Soc. Earthq. Eng. 41, 51–67.

Stirling, M., McVerry, G., Gerstenberger, M., Litchfield, N., Van Dissen, R., Berryman, K., Barnes, P., Wallace, L., Villamor, P., Langridge, R., Lamarche, G., Nodder, S., Reyners, M., Bradley, B., Rhoades, D., Smith, W., Nicol, N., Pettinga, J., Clark, K., Jacobs, K., 2012. National seismic hazard model for New Zealand: 2010 update. Bull. Seismol. Soc. Am. 102, 1514–1542.

Technical Advisory Group on the Santa Cruz Geologic Hazard Investigation, 1991. Geologic hazards in the Summit Ridge area of the Santa Cruz Mountains, Santa Cruz County, California, evaluated in response to the 17 October 1989 Loma Prieta earthquake. Report of Technical Advisory Group: U.S. Geological Survey Open-File Report 91-618, 427 pp.